CHAPTER EIGHTEEN

Spectral deconvolution of electron-bifurcating flavoproteins

Steve Ortiz[a], Dimitri Niks[a], Wayne Vigil Jr[a], Jessica Tran[a], Carolyn E. Lubner[b,*], and Russ Hille[a,*]

[a]Department of Biochemistry, University of California, Riverside, United States
[b]Biosciences Center, National Renewable Energy Laboratory, Golden, CO, United States
*Corresponding authors: e-mail address: cara.lubner@nrel.gov; russ.hille@ucr.edu

Contents

Abstract

Electron-bifurcating flavoproteins catalyze the tightly coupled reduction of high- and low-potential acceptors using a median-potential electron donor, and are invariably complex systems with multiple redox-active centers in two or more subunits. Methods are described that permit, in favorable cases, the deconvolution of spectral changes associated with reduction of specific centers, making it possible to dissect the overall process of electron bifurcation into individual, discrete steps.

Methods in Enzymology, Volume 685
ISSN 0076-6879
https://doi.org/10.1016/bs.mie.2023.03.011

Graphical abstract

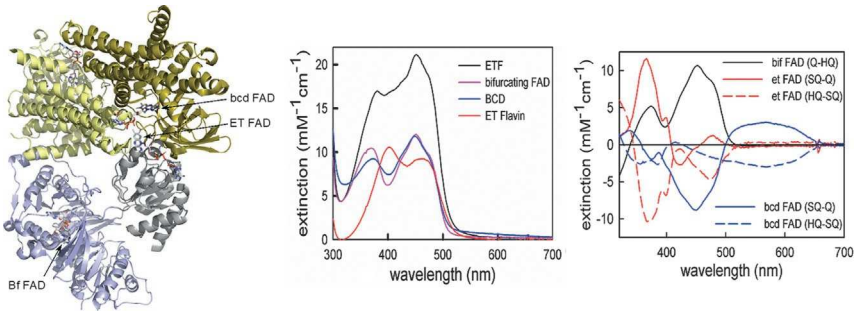

1. Introduction

Flavin-based electron bifurcation involves the two-electron reduction of a flavin site by a median-potential reductant (typically a pyridine nucleotide), followed by transfer of one electron into a high-potential pathway coupled to the transfer of the second electron into a low potential pathway (Buckel & Thauer, 2013, 2018a, 2018b; Herrmann, Jayamani, Mai, & Buckel, 2008; Nitschke & Russell, 2012). While found principally in anaerobic bacteria and archaea, systems utilizing flavin-based electron bifurcation are occasionally also found in aerobes and facultative anaerobes (Poudel et al., 2018). Flavin-based electron transfer is thought to be evolutionarily ancient, some arguing that the Last Universal Common Ancestor to all extant organisms employed flavin-based electron bifurcation (Martin, Bryant, & Beatty, 2018); others have concluded that flavin-based electron bifurcation did not arise until after the divergence of archaea and bacteria and did so independently in different taxa and on multiple occasions (Poudel et al., 2018). Depending on the organism, the low-potential reducing equivalents generated by flavin-based electron bifurcation are used to drive a variety of endergonic processes, including CO_2 and N_2 fixation, H_2 production, methanogenesis, acetogenesis, and the direct generation of transmembrane ion gradients. Electron donors initiating bifurcation include formate in addition to NADH and NADPH. High-potential acceptors include the CoMSSCoB mixed disulfide of methanogens, crotonyl-CoA, caffeyl-CoA, pyruvate, $NAD(P)^+$, menaquinone and ubiquinone, whereas ferredoxins and flavodoxins typically serve as the low-potential

acceptors (Buckel & Thauer, 2013, 2018a, 2018b; Herrmann et al., 2008; Ledbetter et al., 2017).

There are at present 12 different systems demonstrated to utilize flavin-based electron bifurcation. Most of these systems are structurally complex, with two to seven subunits and several redox-active centers (mostly iron-sulfur clusters and flavins but also including hydrogenase-derived FeFe and NiFe H-clusters and molybdenum centers from formate dehydrogenases) in addition to the bifurcating FMN or FAD. The NiFe hydrogenase encoded by the *mvh* operon (Kaster, Moll, Parey, & Thauer, 2011) and the heterodisulfide-linked formate dehydrogenase (Costa et al., 2010), for example, consist of six subunits (some of which participate in both complexes), with a total of 12 and 13 redox-active centers, respectively. The formate dehydrogenase/hydrogenase of *Clostridium autoethanogenum* encoded by the *hyt* operon has seven subunits containing 21 redox-active centers (Wang et al., 2013). There are, however, a few systems that are more amenable to a detailed spectroscopic dissection of the various electron-transfer processes involved in flavin-based electron bifurcation. The first of these is NfnI, an NADH-dependent reduced-ferredoxin:$NADP^+$ oxidoreductase from organisms such as *Thermotoga maritima* and *Pyrococcus furiosus*, which catalyzes the reversible reduction of ferredoxin (the low-potential acceptor) and NAD^+ (the high-potential acceptor) at the expense of NADPH (Demmer, Chowdhury, Selmer, Ermler, & Buckel, 2017; Demmer et al., 2015; Lubner et al., 2017). This dimeric protein has one FAD and a [2Fe-2S] cluster in its smaller subunit, NfnS (also called NfnA), where the FAD is the site of NAD^+ reduction in the high-potential pathway. The [2Fe-2S] cluster has an elevated reduction potential, possibly owing to the substitution of one cysteine residue with an aspartate. The larger NfnL (or NfnB) subunit has a second flavin, L-FAD, which performs NADPH oxidation and the primary bifurcation event, as well as two [4Fe-4S] clusters that constitute the low-potential pathway, with the more distal from the L-FAD being the electron donor to ferredoxin. The physically separated high- and low-potential pathways are thus structurally well-defined in a system containing just five redox-active centers. The overall structure of the *T. maritima* NfnI (Demmer et al., 2015) is shown in Fig. 1.

A second type of more readily studied system catalyzing flavin-based electron bifurcation consists of complexes that possess an electron-transferring flavoprotein (ETF) component. Non-bifurcating ETFs from a variety of both vertebrate and microbial organisms are $\alpha\beta$ dimers, each with one FAD in the α subunit and one AMP in the β subunit. In electron

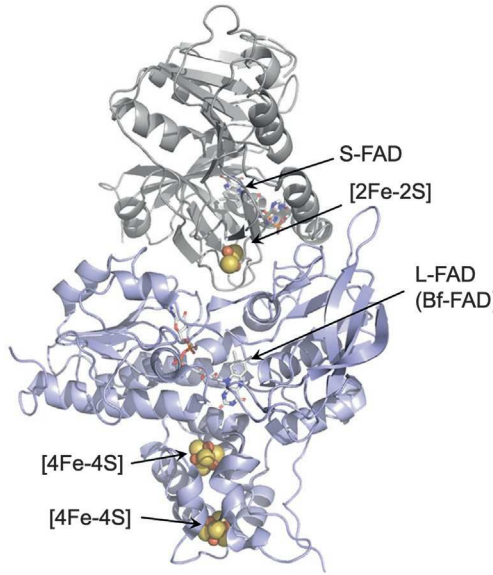

Fig. 1 The structure of NfnI from *Thermotoga maritima* (Demmer et al., 2015); PDB 5OL2. The large subunit is in *blue*, with the bifurcating FAD and two [4Fe-4S] clusters at bottom, and the small subunit in *gray*, with the [2Fe-2S] cluster and NAD^+-reducing FAD at top.

bifurcating ETFs, a second equivalent of FAD is found in place of the AMP in the β subunits, and it is this second FAD that is the primary site of electron bifurcation. This latter FAD is referred to here as the bifurcating FAD (Bf-FAD), and distinct from the first, electron-transferring FAD (ET-FAD). In addition to the dimeric ETF component, these systems have one or two additional subunits that are responsible for reduction of the high-potential substrate (e.g., crotonyl-CoA, caffeyl-CoA, lactate, or menaquinone). In each case, the site of reduction of the high potential substrate occurs at a third equivalent of FAD. The ET-FAD mediates electron transfer between the Bf-FAD and the third FAD as an integral aspect of electron transfer in the high-potential pathway. In the ETF-based systems, there is no low-potential pathway as such, the low-potential ferredoxin substrate simply takes an electron directly from the $Bf\text{-}FAD^{\cdot -}$ formed after the first electron is bifurcated.

The X-ray crystal structures of the isolated EtfAB from the crotonyl-CoA-dependent NADH:ferredoxin oxidoreductase (EtfAB:bcd, for butyryl-CoA dehydrogenase) from *Acidaminococcus fermentans* (Chowdhury et al., 2014) and the complete EtfAB:bcd complex from *Clostridium difficile* (Demmer et al., 2017) are known (Fig. 2A and B). It is clear from a

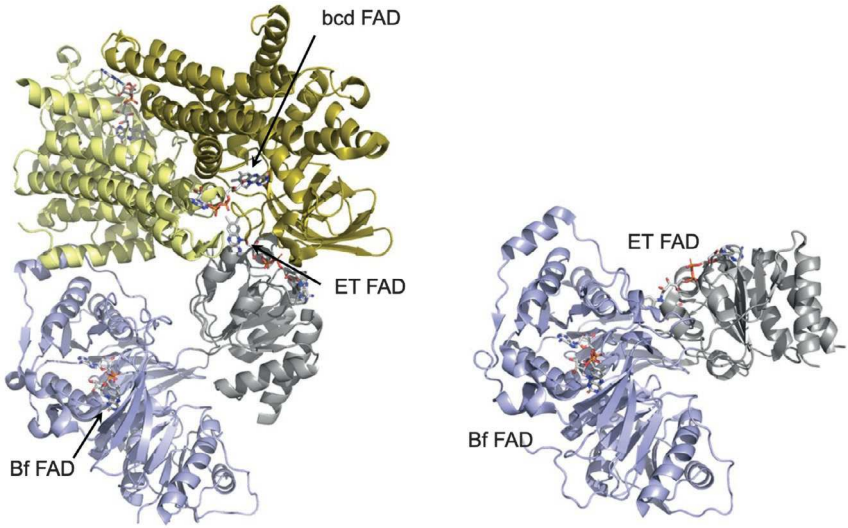

Fig. 2 Structures the EtfAB:bcd complex from *Clostridium difficile* and EtfAB from *Acidaminococcus fermentans* and EtfAB from *A. fermentans* (Chowdhury et al., 2014). *Left*, a protomer of the tetrameric EtfAB:bcd complex from *C. difficile* (Demmer et al., 2017); PDB 5OL2. The EtfAB domain containing the bifurcating FAD is in *blue*, and that containing the electron-transferring FAD is in *gray*. The bcd subunit containing the FAD responsible for reduction of crotonyl-CoA is in *dark yellow*. The overall complex is organized as a dimer of dimers, and the second bcd subunit of the partner dimer is shown in *light yellow* to illustrate the extensive contacts made between the two bcd subunits. *Right*, the EtfAB from *A. fermentans* (Chowdhury et al., 2014); PDB 4KPU. The domains containing the bifurcating and electron-transferring FADs are in *blue* and *gray*, respectively. The orientation is similar to that shown for the *C. difficile* EtfAB:bcd complex to illustrate the significant change in orientation of the domain containing the electron-transferring FAD relative to that containing the bifurcating FAD.

comparison of the structures that the EtfAB domain possessing the ET-FAD rotates dramatically in the course of catalysis from an orientation in which the ET-FAD is proximal to the Bf-FAD to one in which it is proximal to the third FAD found within the bcd subunit (bcd-FAD). This motion, involving a rotation of ~80°, is essential to ensuring transfer of the high-potential electron from the Bf-FAD to the bcd-FAD in the course of bifurcation. This conformational change is in fact a general property of ETFs, and is seen even in those proteins that are not involved in bifurcation (Toogood, Leys, & Scrutton, 2007).

Another ETF-dependent bifurcation system is the EtfABCX menaquinone-dependent NADH:ferredoxin oxidoreductase from organisms such as *Pyrobaculum aerophilum* and *T. maritima* (Fig. 3). The EtfAB component of EtfABCX is very similar to that seen in EtfAB:bcd with Bf- and

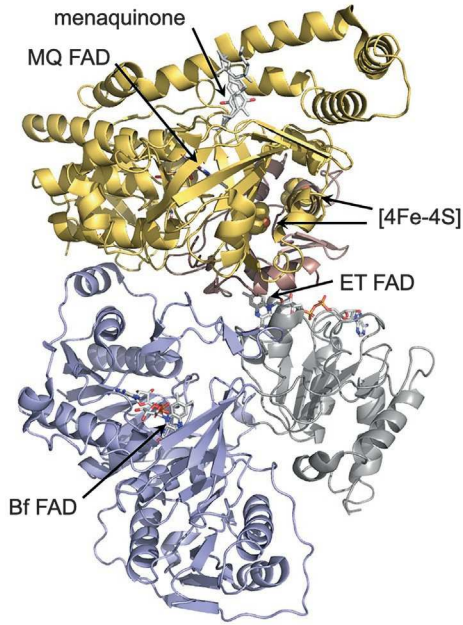

Fig. 3 Structure of EtfABCX from *Thermotoga maritima* (Feng, Schut, Lipscomb, Li, & Adams, 2021); PDB 7KOE. The EtfAB domain containing the bifurcating FAD is in *blue*, and that containing the electron-transferring FAD is in *gray*. The EtfC subunit responsible for reduction of menaquinone, with menaquinone bound, is in *yellow*. The menaquinone-reducing FAD (MQ FAD) is seen edge-on in the orientation shown. The EtfX subunit containing the two [4Fe-4S] clusters is in *red* (in back of the yellow EtfC subunit in the orientation shown).

ET-FADs, although because of differences in gene organization, the subunit designated EtfA in EtfABCX corresponds to EtfB of EtfAB:bcd; similarly, EtfB of EtfABCX corresponds to EtfA of the EtfAB:bcd complex. EtfC possesses a menaquinone-reducing FAD, while EtfX has a pair of [4Fe-4S] clusters, resulting in an overall system that is only moderately more complex than EtfAB:bcd. As shown in Fig. 3, the cryo-electron microscopy structure of EtfABCX has recently been reported (Feng et al., 2021), providing a physical context in which to understand flavin-based electron bifurcation. Interestingly, the two [4Fe-4S] iron-sulfur clusters of EtfX lie between the ET-FAD and the flavin of EtfC as an integral part of the high-potential pathway. This is in contrast with the two [4Fe-4S] clusters of NfnI, which comprise the low-potential pathway in that system. Also, only one of the two [4Fe-4S] clusters in EtfX lie on-path between the two FADs, the second lying off to one side. As in EtfAB:bcd, the low-potential ferredoxin substrate interacts directly with the Bf-FAD of EtfAB.

The thermodynamics of flavin-based electron bifurcation are becoming better understood and take advantage of the fact that flavins (like the simpler quinones) are capable of both one- and two-electron processes (Lubner et al., 2017; Wise et al., 2022; Yuly, Zhang, Lubner, Peters, & Beratan, 2020), with an intermediate one-electron reduced semiquinone state (SQ, as either the neutral $FADH^{\bullet}$ or anionic $FAD^{\bullet-}$) between the oxidized FAD (Q, quinone) and two-electron reduced $FADH_2$ (HQ, which ionizes to $FADH^-$ at neutral pH). The essential aspect of flavin-based electron bifurcation is that the half-potentials of its one-electron Q/SQ and SQ/HQ couples are highly "crossed," or inverted, which occurs when the half-potential for the Q/SQ couple is more negative than that for the SQ/HQ couple. Highly crossed half-potentials result in an extremely low-potential and thus thermodynamically unstable semiquinone state. Subsequent to its two-electron reduction by NAD(P)H, the first electron out of the bifurcating flavin occurs at the higher-potential SQ/HQ couple, leaving behind the low-potential semiquinone whose electron is ultimately passed to the low-potential acceptor. The high- and low-potential electron transfer processes are tightly coupled to one another in the course of steady-state turnover, with little leakage of the low-potential electron to the high-potential acceptor in the course of catalysis (Brereton, Verhagen, Zhou, & Adams, 1998; Chowdhury, Kahnt, & Buckel, 2015; Herrmann et al., 2008; Yuly et al., 2020; Zhang et al., 2017). The central question regarding bifurcation has to do with how this is enabled, i.e., why the low-potential electron generated after the first bifurcated electron transfer from the fully reduced bifurcating site does not simply follow the first electron into the high-potential pathway, a process that must be strongly thermodynamically favorable. The explanation must rely, at least in part, on the kinetics rather than the thermodynamics of the system.

We consider here three specific examples of "simple" bifurcating flavoprotein systems for which structures are available: the NfnI from *P. furiosus*, the EtfAB:bcd from *Megasphaera elsdenii*, and the EtfABCX from *T. maritima*, with a goal of demonstrating how to deconvolute the spectral changes attributable to each of the several discrete electron-transfer events and redox cofactors involved in electron bifurcation.

2. Spectral deconvolution of NfnI

On the basis of the very similar X-ray structures of NfnI from both *T. maritima* (Demmer et al., 2015) and *P. furiosus* (Lubner et al., 2017), it is clear that NfnI has clearly defined high- and low-potential pathways

leading from the central bifurcating FAD (L-FAD) of the large NfnL subunit. The high-potential branch consists of the [2Fe-2S] cluster and the second FAD (S-FAD) of the smaller NfnS subunit and the low-potential pathway consists of the two [4Fe-4S] clusters of NfnL. In principle, deconvolution of the spectral changes associated with each of the steps involved in electron bifurcation are straightforward: an initial reduction of L-FAD from Q to HQ, followed by electron bifurcation to reduce the [2Fe-2S] cluster of the high-potential pathway and the proximal [4Fe-4S] cluster of the low-potential pathway, which together fully reoxidize the L-FAD. Subsequent electron transfer within the high-potential pathway leads to formation of the neutral $FADH^{\cdot}$ species at the S-FAD, which absorbs in the 600 nm region. Each of these steps are expected to be spectroscopically distinct. On the other hand, electron transfer in the low-potential pathway is expected to have a negligible absorbance change in the UV–visible, as it involves electron transfer between the two [4Fe-4S] clusters. This transition, however, can be monitored by freeze-quench EPR, which allows for assessment of the distinct EPR signals of the two [4Fe-4S] clusters (signals that also differ from that of the [2Fe-2S] cluster of the high-potential pathway) (Lubner et al., 2017).

An initial spectroscopic examination of the electron transfer events of electron bifurcation by NfnI utilized ultrafast UV–visible transient absorption spectroscopy (Lubner et al., 2017). Due to the significant oxygen instability of NfnI, all sample preparations were conducted under a nitrogen atmosphere within an MBraun anaerobic chamber. Partial reduction of the NfnI iron-sulfur clusters using sub-stoichiometric amounts of NADPH was performed under these conditions and placed in a screw top and septum-sealed 2 mm quartz cuvette (Firefly Scientific) with micro-stir bar. Low concentrations of NADPH were utilized for enzyme poising because the presence of any unreacted reduced NADPH remaining in the sample was found to be problematic for visualization of the $FAD^{\cdot -}$ species due to overlapping absorptive features. Continuous stirring was employed to ensure no photodegradation during data collection (~35 min). Additionally, the choice of buffer and additives need to be considered for possible UV or vis absorption interference as well as potential photodegradation properties that may interfere with data collection at the desired wavelengths. The protein was excited using a femtosecond pulsed laser (Libra Coherent amplified 4 W Ti:sapphire laser, 800 nm, 1 kHz, 100 fs pulse width) with a pump wavelength of 400 nm to preferentially excite FAD, and the system was coupled with a HELIOS spectrometer (Ultrafast Systems).

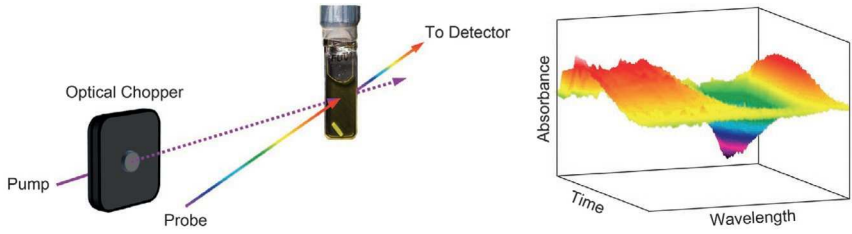

Fig. 4 Schematic of the light pulses utilized in an ultrafast transient absorption experiment (*left*) and a representative plot of the resulting data (*right*). Photochemistry is initiated in the sample by the pump beam which has previously been passed through an optical chopper to remove every other pulse. Changes in the sample are measured by the probe beam which is composed of a white light continuum of wavelengths from ~350–800 nm (when using CaF_2 crystal). It is directed onto the sample at the same position as the pump beam and then passes to a detector, while the pump is blocked. A light-minus-dark absorption spectrum is generated for all wavelengths and a three-dimensional plot is constructed displaying the kinetics at each wavelength in one direction (i.e., the yz plane) and full absorption spectra for each time point in the other direction (i.e., the xy plane).

A schematic of the instrumentation is shown in Fig. 4. A portion of the laser output (fundamental) was utilized to generate a white light continuum after passing through a 2 mm thick CaF_2 crystal. This beam was further split into probe and reference beams. A reference beam was utilized to correct for pulse-to-pulse fluctuations in the white light continuum. Furthermore, the pump beam was modulated by an optical chopper, synchronized with the laser, to block every other pump pulse. Because all probe pulses are detected, half of them measure the sample with the pump beam incident upon it, while the other half measure a non-illuminated sample. This allowed for the generation of a light-minus-dark absorption spectrum. Data was collected at all wavelengths between 350 and 800 nm and from 100 fs to 5 ns time domain, generating 3D plots of spectrophotometric amplitude changes (Fig. 4). This experiment yielded a light-minus-dark difference spectrum with a negative feature at 455 nm and positive feature at 366 nm, indicative of formation of the anionic $FAD^{\cdot -}$ (366 nm) from oxidized FAD (455 nm). Given that S-FAD forms a neutral semiquinone intermediate, the generated anionic semiquinone was attributed to L-FAD. The photochemically generated L-FAD* excited state abstracted an electron from the proximal [4Fe-4S] cluster, the nearer to L-FAD at a distance of 7.5 Å, which upon relaxation to the ground state generated the low-potential $L\text{-}FAD^{\cdot -}$. This subsequently decayed back to oxidized FAD with a lifetime of ~10 ps following electron transfer back to the [4Fe-4S] cluster of the low-potential pathway. As controls, the

laser-induced behavior of NfnI was compared to other flavoproteins that did not bifurcate but were known to form very short lived $FAD^{\bullet -}$ species (Hoben et al., 2017). These were also structurally analyzed for similarity to NfnI, in hopes of establishing whether the observed charge recombination was due to amino acid residues that might have served as electron donor to the photoexcited L-FAD* (e.g., Trp, Tyr, Cys), though none were identified. Thus, decay of $L\text{-}FAD^{\bullet -}$ could be attributed to (back) electron transfer to the proximal [4Fe-4S] cluster and represented the rate of electron transfer between these two species. In addition to the important demonstration that the very low-potential semiquinone of the L-FAD is the anionic $FAD^{\bullet -}$ rather than neutral $FADH^{\bullet}$, the rate constant seen for electron transfer could be used to calculate the driving force for the electron transfer event using the first-principles equation derived by Dutton and coworkers (Page, Moser, Chen, & Dutton, 1999), from which the difference in reduction potentials for donor and acceptor can be calculated. The result is an estimated reduction potential for the Q/SQ couple for the bifurcating FAD of −911 mV, which is very low indeed. This value has been subsequently corroborated through electrochemical investigations of L-FAD and determination of the Q/HQ and SQ/HQ couples (Wise et al., 2022).

In examining the reduction of NfnI by NADPH using stopped-flow spectrophotometry, the kinetics are complicated by the fact that at moderate pH values the reduction potential of the NADPH is not sufficiently low as to fully reduce the protein at modest [NADPH]. As a result, the extent of reduction as well as the observed rate constant increases in proportion to NADPH concentration. While this property has been exploited to poise NfnI in a favorable state for the ultrafast transient absorption experiments described above, it becomes problematic when following the conventional reductive half-reaction. At pH 9 or above, however, the reduction consistently goes to completion with multiphasic kinetics. The fastest portion of the reaction takes place over ~150 ms and appears to involve more than one process. Reduction of the L-FAD must be part of this portion of the reaction, but a small amount of $FADH^{\bullet}$ is also seen at longer wavelengths, which suggests some electron transfer along the high-potential pathway to the S-FAD (*via* the [2Fe-2S] cluster). Formation of the $S\text{-}FADH^{\bullet}$ was confirmed by EPR, with a radical having a 19 G linewidth consistent with formation of *ca.* 10% of the neutral $S\text{-}FADH^{\bullet}$. Reduction of the high potential [2Fe-2S] must also be part of the fast phase reaction, but the observed spectral changes are dominated by the FAD species. On a time scale of ~5 s there is an

additional absorbance increase in the 580–620 nm region, reflecting additional accumulation of S-FADH$^{\bullet}$, while at even longer times (10–30 s), the S-FAD becomes fully reduced, as reflected in a decrease in absorbance in the 580–620 nm region. No spectral changes unambiguously attributable to the [4Fe-4S] clusters of the low-potential pathway are seen in the course of the reaction, although the enzyme does eventually become fully reduced to the level of $NfnI_{6e}-$, with one electron "hole" in the high-potential pathway that resides predominantly on the S-FADH$^{\bullet}$. This result is consistent with previous equilibrium titrations indicating the same (Lubner et al., 2017).

NADH can also be used to reduce NfnI, and the reaction is better behaved than that with NADPH as reductant. The fastest phase of the reaction is complete within 30 ms, and the observed rate constant exhibits hyperbolic dependence on [NADH], yielding a k_{red}^{app} of 205 s^{-1} and K_d^{app} of 29 μM at pH 9.5. There appears to be a lag between the initial reduction of the S-FAD and the subsequent transfer of electrons, presumably to the [2Fe-2S] cluster, which may be due to the inherent kinetics of the electron transfer from the two-electron reduced $FADH_2$ to the [2Fe-2S] cluster being kinetically slow and/or thermodynamically unfavorable to an extent. Over long timescales it can be seen that NfnI becomes more reduced as more electrons travel up the low-potential pathway and reduce the two low-potential [4Fe-4S]. This interpretation assumes that reduction by NADH occurs solely at the S-FAD. In fact, NADH may be able to directly reduce the bifurcating L-FAD as well as the S-FAD, however, a possibility supported by the recent structure of NfnI in complex with NAD^+. While NAD^+ is found bound near the S-FAD in one protomer of the dimeric protein, as expected, in the other protomer of the dimer it is found bound near the bifurcating L-FAD instead. (Fig. 5) (Demmer et al., 2015). Direct reduction of the L-FAD by NADH could explain how the L-FAD is so easily reduced in these experiments. Subsequent to the initial reduction event, regardless of where it takes place, the [4Fe-4S] clusters of the low-potential pathway become reduced over a period of tens of seconds. Neutral semiquinone accumulates at still longer times, consistent with electron transfer between the fully reduced S-FAD and the [2Fe-2S] cluster being slow (since accumulation of the FADH$^{\bullet}$ should occur after the electron transfer to the Fe-S cluster as it leaves behind an electron and a proton on the S-FAD). In addition, over the time course of the reaction at saturating conditions of [NADH] additional flavin reduction occurs as the enzyme becomes fully reduced.

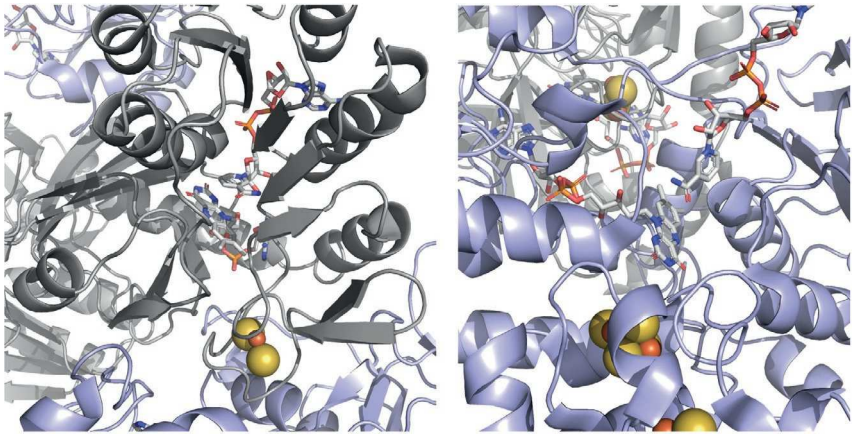

Fig. 5 The structure of NfnI in complex with NAD^+ (Demmer et al., 2015); PDB 4YRY. *Left*, the structure of one protomer within the dimeric protein with NAD^+ bound near the S-FAD, as expected. *Right*, the other protomer within the dimer, however, has NAD^+ bound instead near the bifurcating L-FAD. In both structures, the large subunit is in blue and the small subunit in gray.

3. Spectral deconvolution of EtfAB reduction

The EtfAB:bcd crotonyl-CoA-dependent NADH:ferredoxin oxidoreductase from, e.g., *M. elsdenii*, consists of an EtfAB component with its Bf- and ET-FADs and a butyryl-CoA dehydrogenase component with a third equivalent of FAD (bcd-FAD). Although EtfAB:bcd is an example of the simplest type of bifurcating flavoprotein with only three redox-active centers, spectroscopic analysis is complicated by the fact that all three are flavins. However, there are several factors which have greatly simplified the deconvolution of the spectral changes associated with bifurcation. First, the EtfAB and bcd components can be expressed separately in recombinant systems, making it possible to explicitly assign the absorption spectra of both the oxidized and reduced forms of the bcd component, as well as the spectral change associated with its full reduction to the HQ state (Chowdhury et al., 2015). In addition, the neutral bcdFADH$^{\cdot}$ semiquinone accumulates transiently over the course of reductive titrations of the bcd protein with dithionite, making it possible to deconvolute its absorption spectrum as well.

Another factor that facilitates spectral deconvolution is that the ET-FAD of EtfAB can be readily removed by incubation with KBr, leaving the Bf-FAD, whose absorption spectrum in both the oxidized and fully reduced

forms can then be determined as for the bcd component (Sato, Nishina, & Shiga, 2003; Sato, Nishina, & Shiga, 2013a, 2013b). In addition, the spectral contribution of ET-FAD can be determined from the difference spectra between replete and ET-FAD-depleted protein in both the oxidized and reduced forms. Interestingly, the absorption spectrum obtained for the oxidized ET-FAD exhibits a significant red shift of the flavin absorption envelope that typically exhibits an absorption maximum around 360 nm. The several discrete electronic transitions contributing to this absorption envelope have been shown to possess significant charge-transfer character within the isoalloxazine ring, making them particularly sensitive to the protein environment (Kar, Miller, & Mroginski, 2022). Empirically, this translates to the oxidized forms of Bf-FAD and ET-FAD in EtfAB being more easily distinguishable from one another than would otherwise be expected.

The final factor facilitating spectral deconvolution is the fact that, as with the non-bifurcating ETFs containing only the ET-FAD and an AMP in place of Bf-FAD, the ET-FAD of EtfAB forms a particularly stable anionic $FAD^{\bullet -}$ in the course of reductive titrations with dithionite, and this is the highest-potential cofactor in the protein. As with the neutral $FADH^{\bullet}$ seen with the bcd-FAD, the absorption spectrum of the ET-$FAD^{\bullet -}$ can be deconvoluted from spectra seen in the course of dithionite titrations. It is worth noting that while a pair of reducing equivalents are ultimately required to reduce the high-potential crotonyl-CoA substrate, electrons are introduced one at a time into the high-potential pathway. That the ET-FAD forms the anionic $FAD^{\bullet -}$ while the bcd-FAD forms the neutral $FADH^{\bullet}$ makes it particularly straightforward to follow the individual electron-transfer events associated with bifurcation in these systems, underscoring the utility of the approach. Fig. 6 summarizes the absorption spectra and difference spectra seen for each of the three equivalents of FAD found in EtfAB:bcd (Vigil et al., 2021).

Under normal conditions, the Bf-FAD of EtfAB is expected to have extremely crossed half-potentials, meaning again that the semiquinone of this cofactor cannot accumulate to any significant degree in the course of reductive titrations. While reductive titrations of the *M. elsdenii* EtfAB depleted of ET-FAD with NADH show a monotonic spectral change from oxidized to reduced protein. Unusually for these ETFs, no long-wavelength absorption attributable to an $ETF_{red}{}^{\bullet}NAD^{+}$ charge-transfer complex is observed. By contrast, titrations with sodium dithionite result in the near-quantitative accumulation of an anionic $FAD^{\bullet -}$ (Vigil et al., 2021). The differing behavior in the NADH and dithionite titrations is a reflection of the

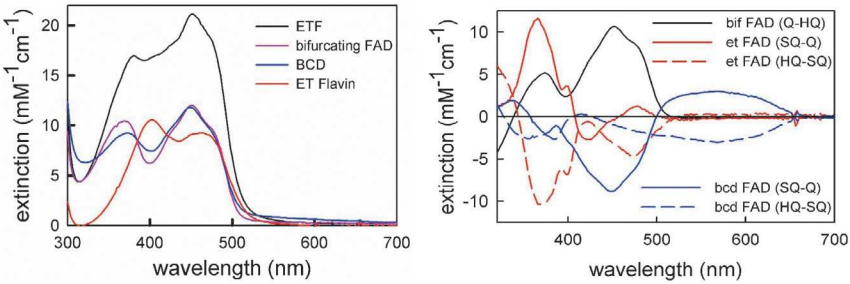

Fig. 6 Spectral deconvolution the spectral contributions of the three FADs of EtfAB:bcd. *Left*, absorption spectra of: replete EtfAB (*black*); The spectrum of oxidized EtfAB depleted of the electron-transferring FAD, yielding the spectrum of the bifurcating FAD (*magenta*); the spectrum of the oxidized electron-transferring FAD, obtained by subtracting the spectrum of the bifurcating FAD from that for replete EtfAB (*red*); as-isolated oxidized bcd (*blue*). *Right*, difference spectra seen upon reduction of each flavin (two-electron for the bifurcating FAD, sequential one-electron reduction in the case of the electron-transferring and bcd flavins).

fact that NADH is an obligatory two-electron donor while dithionite (actually $SO_2^{\bullet-}$ in aqueous solution) is a one-electron donor. The observation of such large accumulation of $FAD^{\bullet-}$ in the course of the dithionite titrations with the ET-FAD-depleted EtfAB, where the only flavin remaining in the protein is the Bf-FAD, implies that removal of the ET-FAD results in a dramatic uncrossing of the Bf-FAD half-potentials. This is an important point as discussed further below in the context of the kinetics of EtfAB reduction by NADH. The depleted *M. elsdenii* EtfAB is rapidly reduced by NADH, the dependence of k_{obs} on [NADH] is hyperbolic, with K_d and limiting k_{red} values of 96 μM and 1600 s^{-1}.

It is clear from the endpoint absorption spectrum seen in equilibrium titrations of replete EtfAB with NADH that full reduction of both the Bf- and ET-FADs has occurred (Sato et al., 2013a, 2013b; Vigil et al., 2022), meaning that the low-potential electron in the transiently generated Bf $FAD^{\bullet-}$ ultimately migrates to the ET FAD (required before the Bf FAD can react with a second equivalent of NADH). That reduction goes to completion implies that in the absence of ferredoxin the low-potential electron generated in the course of the reaction of protein with the first equivalent of NADH must eventually make its way to the ET-FAD in the high-potential pathway (as expected on thermodynamic grounds) before a second equivalent of NADH can react with the now fully reoxidized Bf-FAD to result in full reduction of the protein. Indeed, the kinetics of the reaction of replete EtfAB with NADH is markedly multiphasic, with a fast phase going to completion within 20 ms, an intermediate phase taking place on a time scale

of hundreds of ms and a slow phase that goes to completion in ~100 s (Vigil et al., 2022). The fast phase exhibits a hyperbolic dependence on [NADH], yielding $k_{red} = 590\,s^{-1}$ and $K_d = 30\,\mu M$, and accounts for approximately 50% of the total absorbance change at 450 nm. A comparison with the reaction of NADH with EtfAB depleted of ET-FAD clearly demonstrates that this fast phase reflects the initial reduction of the Bf-FAD and formation of the intermediate $EtfAB_{2e}-$ species with a fully reduced Bf-FAD HQ. The slower two phases are independent of [NADH] and reflect intramolecular processes. The intermediate phase contributes only minimally to the spectral change at 450 nm but is associated with a large absorbance increase at 370 nm that reflects extensive accumulation of $FAD^{\cdot -}$ on the time scale of 100 ms. This phase is considered further below. The slowest phase of the reaction results in full reduction of the EtfAB and can be assigned to the reaction with a second equivalent of NADH once the Bf-FAD has been reoxidized by (rate-limiting) intramolecular electron transfer to give fully reduced ET-FAD HQ. It is this last step that is rate-limited by the "leakage" of a low-potential electron into the high-potential pathway (of which transfer to the ET-FAD is the first step). A schematic of the several processes involved is given in Fig. 7.

The accumulation of $FAD^{\cdot -}$ in the intermediate phase of the reaction of EtfAB with NADH requires additional comment. In principle, this could arise from intermolecular electron transfer between two $EtfAB_{2e}-$ molecules to give one equivalent each of $EtfAB_{1e}-$ and $EtfAB_{3e}-$, both of which would be expected to have the ET-FAD as $FAD^{\cdot -}$ since this is the highest potential in the system. In fact, however, intermolecular electron transfer takes place on a time scale of several 100 s and is slower even that the slowest

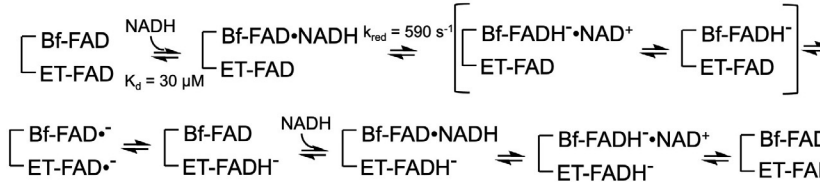

Fig. 7 A schematic of the discrete events associated with the reduction of EtfAB by NADH. NADH binding and reduction of the bifurcating FAD is followed by establishment of an equilibrium between two electron distribution, one with a single electron on each flavin, and a second with the electron-transferring FAD fully reduced. Protein in the latter distribution is able to react with a second equivalent of NADH to yield the fully reduced protein. The two bracketed intermediates are not seen as discrete species with the *Megasphaera elsdenii* EtfAB, but are seen as long-wavelength absorbing charge-transfer complexes with the *A. fermentans* and *T. maritima* EtfABs.

phase seen in the reaction of EtfAB with NADH (Vigil et al., 2022), meaning that whatever is happening in the intermediate phase of the reaction with NADH is occurring within $EtfAB_{2e}-$. The unavoidable conclusion is that if one of the flavins in $EtfAB_{2e}-$ is present as the semiquinone the other must be also. To the extent that the Bf-$FAD^{\cdot -}$ accumulates during this phase of the reaction the implication is that its potentials must have become uncrossed (as is seen on removal of the ET-FAD). From the extent of the absorbance increase seen at 370 nm, it is estimated that some 20% of $EtfAB_{2e}-$ exists in the election distribution with both bifurcating and electron transferring flavins as $FAD^{\cdot -}$ (Vigil et al., 2022). It has been suggested that the crystallographically established structural reorientation of the domain containing the ET-FAD (Demmer et al., 2017) is involved in the observed uncrossing of the Bf-FAD's half-potentials, but it remains for future work to establish whether uncrossing occurs normally in the course of bifurcating turnover in this and other systems.

The EtfAB components of EtfABCX from both *P. aerophilum* and *T. maritima* behave very similarly to that seen from the *M. elsdenii* EtfAB, including the ease of removing the ET-FAD, facilitating the spectral assignments of the two flavins, and uncrossing the Bf-FAD half-potentials upon doing so; one difference in behavior is that the *P. aerophilum* protein exhibits a strong $Ered^{\cdot}NAD^{+}$ charge-transfer complex at completion of titrations with NADH (Vigil et al., 2022). The reaction of the *P. aerophilum* EtfAB depleted of its ET-FAD is cleanly monophasic, with a hyperbolic dependence of the observed rate of reduction on [NADH], yielding K_d and k_{red} values of 75 μM and 930 s^{-1}, respectively, quite similar to what is seen with the *M. elsdenii* protein. Similarly, reaction of the replete *P. aerophilum* EtfAB with an excess of NADH is multiphasic. The wavelength dependence of the fastest (and [NADH]-dependent) phase is consistent with the initial reduction of the Bf-FAD to HQ, with concomitant formation of a long wavelength-absorbing charge-transfer complex between the reduced Bf-FAD HQ and NAD^{+}. The amount of the intermediate $EtfAB_{2e}-$ present in the distribution with two $FAD^{\cdot -}$ at the end of the intermediate phase of the reaction is some 40%, even greater than seen with the *M. elsdenii* EtfAB s (Vigil et al., 2022).

4. Prospectus

Ongoing work with NfnI focuses on further deconvolution of the individual steps of electron transfer along the high-potential pathway to the S-FAD, and examining the effectiveness of ferredoxin reduction of

NADPH-reduced enzyme in the absence of NAD^+. An additional goal is to identify those steps that might involve proton-coupled electron transfer (such as electron transfer from the fully reduced L-$FADH^-$ to the [2Fe-2S] cluster of the high-potential pathway, leaving the L-$FAD^{\cdot -}$, and from the [2Fe-2S] cluster to the S-FAD in the high-potential pathway, which entails reduction of the S-FAD to the neutral $FADH^{\cdot}$ semiquinone). Such studies will be greatly facilitated by the distinct spectroscopic features identified here that are associated with each discrete electron transfer event.

With electron transfer within EtfAB from two distinct systems thus characterized, future work will examine the individual electron transfer steps in the high-potential pathway of the intact EtfAB:bcd and EtfABCX complexes. With each primary bifurcation event, a high-potential electron is expected to be transferred to the ET-FAD, forming a thermodynamically stable anionic semiquinone, leaving behind a low-potential electron at the Bf-$FAD^{\cdot -}$ that can reduce ferredoxin. In the absence of ferredoxin, a low-potential electron must eventually leak into the high-potential pathway, following the high-potential electron, as reflected in the fact that reductive titrations with NADH in the absence of ferredoxin lead to full reduction of both EtfAB:bcd and EtfABCX. Electron transfer along the high-potential pathway in EtfAB:bcd should be relatively straightforward to deconvolute in the former case given the distinct spectral changes associated with each of the three FADs, as illustrated in Fig. 6. In the case of EtfABCX, electron transfer along the high-potential pathway should be facilitated by the fact that at least the one on-path iron-sulfur cluster, with its absorption change on reduction distinct from that of the flavins in the system, is intervening between the ET-FAD of the EtfAB component and the menaquinone-reducing FAD of the complex. In this way, it should be possible to obtain a more complete picture of the kinetic behavior of these systems and hopefully identify those features that are critical for electron bifurcation.

Acknowledgments

Work in the authors' laboratories was supported by the Department of Energy (DE-SC00010666 to RH), the National Institutes of Health (GM 135088 to RH) and the National Science Foundation (CHE 2101672 to RH). CEL is the recipient of an award from the Early Career Research Program of the Office of Science, Department of Energy. This work was authored in part by the National Renewable Energy Laboratory, operated by Alliance for Sustainable Energy, LLC, for the U.S. Department of Energy (DOE) under Contract No. DE-AC36-08GO28308 with funding provided by the U.S. DOE Office of Science to CEL. The views expressed in the article do not necessarily

Declaration of interests

*Please **tick** the appropriate statement below (please do not delete either statement) and declare any financial interests/personal relationships which may affect your work in the box below.*

☒ The authors declare that they have no known competing financial interests or personal relationships that could have appeared to influence the work reported in this paper.

Ethics statements

N/A

CRediT author statement

CRediT is an initiative that enables authors to share an accurate and detailed description of their diverse contributions to a published work.

Example of a CRediT author statement

***Steve Ortiz:** Contributed writing and figure preparation on NfnI; **Dimitri Niks**: Contributed writing and figure preparation. **Wayne Vigil, Jr.**: Contributed writing and figure preparation for EtfAB:bcd. **Jessica Tran:** Contributed writing and figure preparation for EtfABCX. **Carolyn E. Lubner**: Contributed writing and figure preparation; initiated TAS NfnI project.: **Russ Hille:** Contributed writing and figure preparation; initiated EtfAB:bcd and EtfABCX projects.*

Supplementary material and/or additional information

N/A

References

Brereton, P. S., Verhagen, M., Zhou, Z. H., & Adams, M. W. W. (1998). Effect of iron--sulfur cluster environment in modulating the thermodynamic properties and biological function of ferredoxin from *Pyrococcus furiosus*. *Biochemistry*, *37*(20), 7351–7362. https://doi.org/10.1021/bi972864b.

Buckel, W., & Thauer, R. K. (2013). Energy conservation *via* electron bifurcating ferredoxin reduction and proton/Na + translocating ferredoxin oxidation. *Biochimica et Biophysica Acta-Bioenergetics*, *1827*(2), 94–113. https://doi.org/10.1016/j.bbabio.2012.07.002.

Buckel, W., & Thauer, R. K. (2018a). Flavin-based electron bifurcation, a new mechanism of biological energy coupling. *Chemical Reviews*, *118*(7), 3862–3886. https://doi.org/10.1021/acs.chemrev.7b00707.

Buckel, W., & Thauer, R. K. (2018b). Flavin-based electron bifurcation, ferredoxin, flavodoxin, and anaerobic respiration with protons (Ech) or NAD(+) (Rnf) as electron acceptors: A historical review. *Frontiers in Microbiology*, *9*, 1–26. https://doi.org/10.3389/fmicb.2018.00401.

Chowdhury, N. P., Kahnt, J., & Buckel, W. (2015). Reduction of ferredoxin or oxygen by flavin-based electron bifurcation in Megasphaeraelsdenii. *FEBS Journal*, *282*(16), 3149–3160. https://doi.org/10.1111/febs.13308.

Chowdhury, N. P., Mowafy, A. M., Demmer, J. K., Upadhyay, V., Koelzer, S., Jayamani, E., et al. (2014). Studies on the mechanism of electron bifurcation catalyzed by electron transferring flavoprotein (Etf) and butyryl- CoA dehydrogenase (Bcd) of *Acidaminococcus fermentans*. *Journal of Biological Chemistry*, *289*(8), 5145–5157. https://doi.org/10.1074/jbc.M113.521013.

Costa, K. C., Wong, P. M., Wang, T., Lie, T. J., Dodsworth, J. A., Swanson, I., et al. (2010). Protein complexing in a methanogen suggests electron bifurcation and electron delivery from formate to heterodisulfide reductase. *Proceedings of the National Academy of Sciences of the United States of America*, *107*(24), 11050–11055. https://doi.org/10.1073/pnas.1003653107.

Demmer, J. K., Chowdhury, N. P., Selmer, T., Ermler, U., & Buckel, W. (2017). The semiquinone swing in the bifurcating electron transferring flavoprotein/butyryl-CoA dehydrogenase complex from *Clostridium difficile*. *Nature Communications*, *8*, 1–10. https://doi.org/10.1038/s41467-017-01746-3.

Demmer, J. K., Huang, H., Wang, S. N., Demmer, U., Thauer, R. K., & Ermler, U. (2015). Insights into flavin-based electron bifurcation *via* the NADH-dependent reduced ferredoxin:NADP oxidoreductase structure. *Journal of Biological Chemistry*, *290*(36), 21985–21995. https://doi.org/10.1074/jbc.M115.656520.

Feng, X., Schut, G. J., Lipscomb, G. L., Li, H. L., & Adams, M. W. W. (2021). Cryoelectron microscopy structure and mechanism of the membrane-associated electron-bifurcating flavoprotein Fix/EtfABCX. *Proceedings of the National Academy of Sciences of the United States of America*, *118*(2), e2016978118. https://doi.org/10.1073/pnas.2016978118.

Herrmann, G., Jayamani, E., Mai, G., & Buckel, W. (2008). Energy conservation *via* electron-transferring flavoprotein in anaerobic bacteria. *Journal of Bacteriology*, *190*(3), 784–791. https://doi.org/10.1128/jb.01422-07.

Hoben, J. P., Lubner, C. E., Ratzloff, M. W., Schut, G. J., Nguyen, D. M. N., Hempel, K. W., et al. (2017). Equilibrium and ultrafast kinetic studies manipulating electron transfer: A short-lived flavin semiquinone is not sufficient for electron bifurcation. *Journal of Biological Chemistry*, *292*(34), 14039–14049. https://doi.org/10.1074/jbc.M117.794214.

Kar, R. K., Miller, A. F., & Mroginski, M. A. (2022). Understanding flavin electronic structure and spectra. *Wiley Interdisciplinary Reviews: Computational Molecular Science*, *12*(2), 1–22. https://doi.org/10.1002/wcms.1541.

Kaster, A.-K., Moll, J., Parey, K., & Thauer, R. K. (2011). Coupling of ferredoxin and heterodisulfide reduction *via* electron bifurcation in hydrogenotrophic methanogenic archaea. *Proceedings of the National Academy of Sciences of the United States of America*, *108*(7), 2981–2986. https://doi.org/10.1073/pnas.1016761108.

Ledbetter, R. N., Costas, A. M. G., Lubner, C. E., Mulder, D. W., Tokmina-Lukaszewska, M., Artz, J. H., et al. (2017). The electron bifurcating FixABCX protein complex from *Azotobacter vinelandii*: Generation of low-potential reducing equivalents for nitrogenase catalysis. *Biochemistry*, *56*(32), 4177–4190. https://doi.org/10.1021/acs.biochem.7b00389.

Lubner, C. E., Jennings, D. P., Mulder, D. W., Schut, G. J., Zadvornyy, O. A., Hoben, J. P., et al. (2017). Mechanistic insights into energy conservation by flavin-based electron bifurcation. *Nature Chemical Biology*, *13*(6), 655. https://doi.org/10.1038/nchembio.2348.

Martin, W. F., Bryant, D. A., & Beatty, J. T. (2018). A physiological perspective on the origin and evolution of photosynthesis. *FEMS Microbiology Reviews*, *42*(2), 205–231. https://doi.org/10.1093/femsre/fux056.

Nitschke, W., & Russell, M. J. (2012). Redox bifurcations: Mechanisms and importance to life now, and at its origin. *BioEssays*, *34*(2), 106–109. https://doi.org/10.1002/bies.201100134.

Page, C. C., Moser, C. C., Chen, X. X., & Dutton, P. L. (1999). Natural engineering principles of electron tunnelingtunnelling in biological oxidation-reduction. *Nature*, *402*(6757), 47–52. Retrieved from ://WOS:000083638600036.

Poudel, S., Dunham, E. C., Lindsay, M. R., Amenabar, M. J., Fones, E. M., Colman, D. R., et al. (2018). Origin and evolution of flavin-based electron bifurcating enzymes. *Frontiers in Microbiology*, *9*, 1–26. https://doi.org/10.3389/fmicb.2018.01762.

Sato, K., Nishina, Y., & Shiga, K. (2003). Purification of electron-transferring flavoprotein from *M. elsdeniiMegasphaera elsdenii* and binding of additional FAD with an unusual absorption spectrum. *Journal of Biochemistry*, *134*(5), 719–729. https://doi.org/10.1093/jb/mvg199.

Sato, K., Nishina, Y., & Shiga, K. (2013a). Decomposition of the fluorescence spectra of two FAD molecules in electron-transferring flavoprotein from *Megasphaera elsdenii*. *Journal of Biochemistry*, *154*(1), 61–66. https://doi.org/10.1093/jb/mvt027.

Sato, K., Nishina, Y., & Shiga, K. (2013b). Interaction between NADH and electron-transferring flavoprotein from *Megasphaera elsdenii*. *Journal of Biochemistry*, *153*(6), 565–572. https://doi.org/10.1093/jb/mvt026.

Toogood, H. S., Leys, D., & Scrutton, N. S. (2007). Dynamics driving function - new insights from electron transferring flavoproteins and partner complexes. *FEBS Journal*, *274*(21), 5481–5504. https://doi.org/10.1111/j.1742-4658.2007.06107.x.

Vigil, W., Jr., Niks, D., Franz-Badur, S., Chowdhury, N., Buckel, W., & Hille, R. (2021). Spectral deconvolution of redox species in the crotonyl-CoA-dependent NADH:ferredoxin oxidoreductase from *Megasphaera elsdenii*. A flavin-dependent bifurcating enzyme. *Archives of Biochemistry and Biophysics*, *701*, 108793. https://doi.org/10.1016/j.abb.2021.108793.

Vigil, W., Tran, J., Niks, D., Schut, G. J., Ge, X. X., Adams, M. W. W., et al. (2022). The reductive half-reaction of two bifurcating electron-transferring flavoproteins: Evidence for changes in flavin reduction potentials mediated by specific conformational changes. *Journal of Biological Chemistry*, *298*(6), 1–12. https://doi.org/10.1016/j.jbc.2022.101927.

Wang, S. N., Huang, H. Y., Kahnt, J., Mueller, A. P., Kopke, M., & Thauer, R. K. (2013). NADP-specific electron-bifurcating FeFe -hydrogenase in a functional complex with formate dehydrogenase in clostridium autoethanogenum grown on CO. *Journal of Bacteriology*, *195*(19), 4373–4386. https://doi.org/10.1128/jb.00678-13.

Wise, C. E., Ledinina, A. E., Mulder, D. W., Chou, K. J., Peters, J. W., King, P. W., et al. (2022). An uncharacteristically low-potential flavin governs the energy landscape of electron bifurcation. *Proceedings of the National Academy of Sciences of the United States of America*, *119*(12), 1–6. https://doi.org/10.1073/pnas.2117882119.

Yuly, J. L., Zhang, P., Lubner, C. E., Peters, J. W., & Beratan, D. N. (2020). Universal free-energy landscape produces efficient and reversible electron bifurcation. *Proceedings of the National Academy of Sciences of the United States of America*, *117*(35), 21045–21051. https://doi.org/10.1073/pnas.2010815117.

Zhang, P., Yuly, J. L., Lubner, C. E., Mulder, D. W., King, P. W., Peters, J. W., et al. (2017). Electron bifurcation: Thermodynamics and kinetics of two-electron brokering in biological redox chemistry. *Accounts of Chemical Research*, *50*(9), 2410–2417. https://doi.org/10.1021/acs.accounts.7b00327.